Fusion Engineering and Design 146 (2019) 850–853

Contents lists available at ScienceDirect

Fusion Engineering and Design

journal homepage: www.elsevier.com/locate/fusengdes

Heavy ion beam probe design and operation on the T-10 tokamak

A.V. Melnikov[a,b,c,*], M.A. Drabinskiy[a,c], L.G. Eliseev[a], P.O. Khabanov[a,c], N.K. Kharchev[a], L.I. Krupnik[d], J.L. De Pablos[e], A.S. Kozachek[d], S.E. Lysenko[a], A. Molinero[e], G.B. Igonkina[a], M.M. Sokolov[a]

[a] NRC 'Kurchatov Institute', 123182, Moscow, Russia
[b] NRNU MEPhI, 115409, Moscow, Russia
[c] Moscow Institute of Physics and Technology, 141700, Dolgoprudny, Moscow Region, Russia
[d] Institute of Plasma Physics, KIPT, 310108, Kharkov, Ukraine
[e] Fusion National Laboratory, CIEMAT, 28040, Madrid, Spain

ARTICLE INFO

Keywords:
Heavy ion beam probe
Plasma potential
Turbulent particle flux
Rotation
Geodesic acoustic modes

ABSTRACT

Advanced heavy ion beam probe (HIBP) operates on the T-10 tokamak with 20–130 μA Tl^+ beam accelerated up to 330 keV. The HIBP has a unique capability to measure the mean value of the core plasma potential, and the oscillations in potential φ, density n_e and poloidal magnetic field simultaneously in 5 spatially separated sample volumes for OH and ECRH plasmas with $\tilde{n}_e = (0.3 - 5) \times 10^{19}\,m^{-3}$, $100 < I_{pl} < 330$ kA. Time evolution of local plasma parameters and/or radial profiles can be measured in a single shot. The profile in the range $0.25 < \rho < 1$ is available shot by shot for $B_0 < 2.2$ T. The paper describes main elements of hardware: injector, beamlines, control systems, analyzer, power supplies, and software for HIBP. Physical examples show that HIBP can measure the cross-phase of density oscillations, the poloidal phase velocity of turbulence rotation, the poloidal electric field and the radial turbulent particle flux. Spectral analysis allows us to distinguish various types of turbulence, such as broadband (< 500 kHz), quasicoherent, tearing and geodesic acoustic modes.

1. Introduction

Electric field is considered as an important parameter affecting the turbulent energy and particle transport in toroidal fusion plasmas [1, 2]. Heavy ion beam probe (HIBP) is a unique diagnostics to measure the core electric potential in magnetically confined fusion plasma, for tokamaks, as reviewed in [3], and stellarators [4–6]. The schematic of HIBP is shown in Fig. 1.

A singly charged Tl^+ primary beam with an energy E_b up to 330 keV is injected into the plasma in the vertical plane, the doubly charged secondary ions Tl^{++}, ionized due to collisions with plasma particles, are registered by the energy analyzer, located outside the plasma [7]. Direct and local measurements of plasma potential [8, 9] are obtained by the difference in energies between the secondary and primary probing particles: $\varphi = (E_d - E_b)/e$, where E_d is measured by a position-sensitive split-plate beam detector (pt. 7 in Fig. 1). HIBP also gives information about the oscillations of the electron density n_e by the secondary beam current I_{tot} and the poloidal magnetic field B_{pol} by toroidal beam position $\delta z_d(t)$ [3, 10]. The detector is designed for simultaneous measurements of all three parameters aiming for comprehensive analysis of the plasma turbulence.

The present paper is focused in the compact HIBP design and technology, allowing to measure plasma parameters from the core to the edge within the whole operational limits of T-10 [11].

2. HIBP hardware

2.1. Ion beam injector

The injector provides extracting, focusing and accelerating of primary Tl^+ ion beam for plasma probing. Thermo-ionic solid-state emitter heated up to 800–1200 °C extracts ion current from its surface [12]. An extractor voltage (< 10 kV) takes out the ions from emitter surface, while the focusing voltage (< 10 kV) forms the fine-focused beam. Single ended electrostatic accelerator increases the beam energy E_b up to several hundred kilovolts.

The beam emitter (Fig. 2) is a replaceable element in the emitter-extractor unit with a finite lifetime and capacity about 2 mA × h. For stable operation a new emitter must be degassed through the gradual training heating in the vacuum with pressure control.

* Corresponding author at: NRC 'Kurchatov Institute', 123182, Moscow, Russia.
E-mail address: Melnikov_AV@nrcki.ru (A.V. Melnikov).

https://doi.org/10.1016/j.fusengdes.2019.01.096
Received 26 September 2018; Received in revised form 21 December 2018; Accepted 21 January 2019
Available online 23 January 2019
0920-3796/

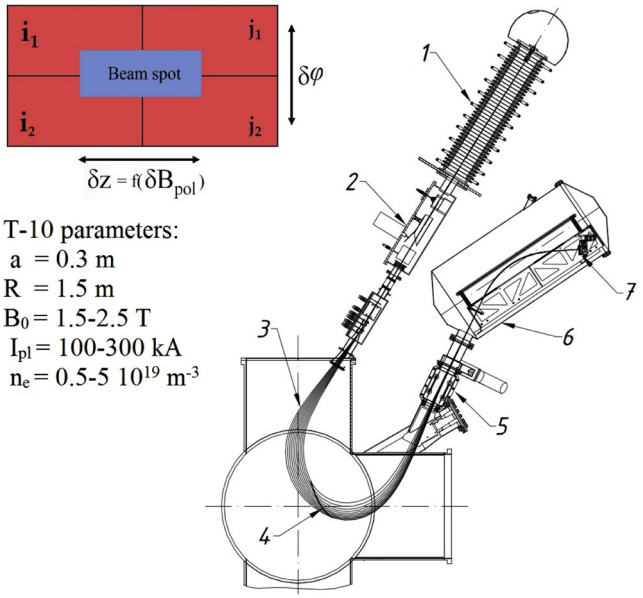

Fig. 1. HIBP diagnostic on T-10: 1–Tl^+ beam injector; 2-primary beamline; 3-primary trajectory; 4-detector line (fat curve); 5-secondary beamline; 6-energy analyzer; 7–beam detector; Inset: currents i_1, i_2, j_1, j_2 to the split-plate beam detector allow simultaneous measurements of the potential, density and poloidal magnetic field in the single sample volume (SV).

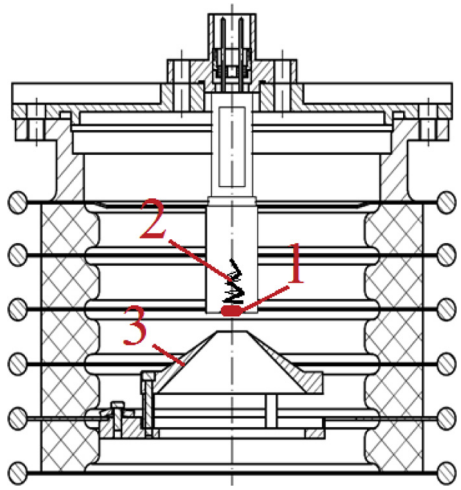

Fig. 2. Emitter-extractor unit: 1–thermo-ionic emitter, 2–heating filament, 3–extracting electrode.

Design of the emitter-extraction unit provides a fine axial alignment of the emitter and extractor electrode and absence of the electrical breakdown. The accelerator is equipped with the anti-corona conductor and guard rings to avoid corona discharge and electrical breakdown.

2.2. Primary and secondary beamlines

Primary beamline (Fig. 3) serves to transport the beam from the accelerator to the plasma and to adjust the entrance angles. The α_1 plates correct misalignment between accelerator and primary beamline in the vertical plane. The poloidal sweeping angle is set up by α_2 plates, nearest to the plasma; β_1 and β_2 plates serve to compensate the beam toroidal shift caused by plasma current. Due to the limited toroidal size of the entrance port (vertical port in Fig. 1) a zig-zag schematic is used. Two wire sensors, altogether with the third one, located inside the vertical port, are used to control the beam focusing by measuring the beam size and position. The primary beamline is not sufficient to

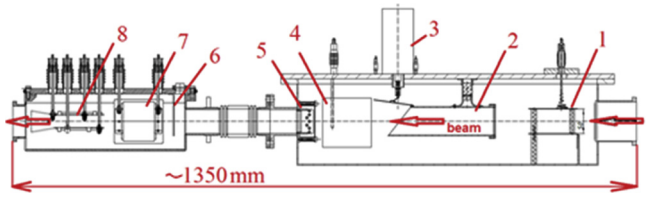

Fig. 3. Primary beamline: deflector plates: 1 - α_1, 2 - β_1, 3 - β_2, 4 - α_2, 5 - Faraday cup, 6 – magnetic driven baffle, 7, 8 - wire sensors.

compensate the toroidal shift, so the secondary beamline (pt. 5 in Fig. 1) was applied [13]. The poloidal sweeping by α_3 plates provides the tuning of the analyzer entrance angle θ_i, while β_3 plates, located inside the vacuum chamber, additionally compensate toroidal shift of the secondary particles. The correcting plates α_2, α_3, β_2, β_3, located close to plasma, are heated up to 200 °C to avoid carbon film formation, which causes the high-voltage breakdown. Heating is realized via insulating transformers with secondary winding under correcting voltage. Heating circuit is cut-off at the start of the discharge to avoid the plate deformation due to the electromagnetic forces caused by current induction during magnetic field pulse.

2.3. Real-time control of toroidal beam shift

The feedback system for toroidal correction of the secondary trajectories by variation of the voltage on β_3 correcting plates uses the beam toroidal position in the detector δz_d (see Fig. 1) as an input signal.

The real-time control system (based on STM-32 microcontroller) allows routine HIBP operation in the regimes with plasma current ramp-up or ramp-down, including initial stage of the discharge. Fig. 4 compares $\delta z_d(t)$ signals in discharges with and without feedback. Feedback keeps the beam near the centre of the detector $\delta z_d(t) < 0.5$ avoiding the signal loss during the whole discharge duration.

2.4. Energy analyzer

The parallel-plate ion energy analyzer [14] provides the measurement of the secondary ion beam energy with a high resolution ($\Delta E_b/E_b < 5\times 10^{-5}$), it operates with anode voltage $U_a < 75$ kV. The secondary beam energy is given by $E_d = 2U_a(F(\theta_i)\delta i + G(\theta_i))$, where F is dynamic factor, G – gain, $\delta i = \frac{i_1+j_1-i_2-j_2}{i_1+j_1+i_2+j_2}$, see Fig.1.

The analyzer (Fig. 5) has five 2-mm entrance slits allowing simultaneous measurements in five different SVs with a size < 1 cm^3. The anode high-voltage plate has a hole to prevent the reflection of the plasma light to the beam detector, so to avoid the parasitic current caused by secondary electrons. This hole is covered by the wire grid to

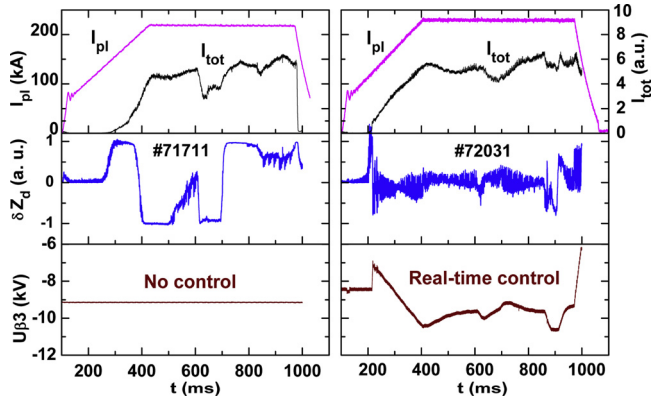

Fig. 4. Time traces of plasma current I_{pl}, secondary beam current I_{tot}, beam toroidal position in the detector δz_d and voltage on β_3 correcting plates for the shots with and without real-time control system of beam toroidal shift.

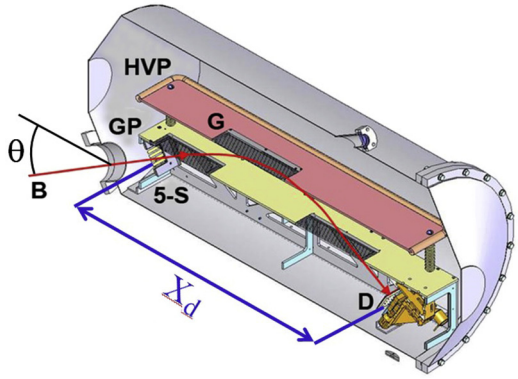

Fig. 5. Energy analyzer: B - secondary particle trajectory, 5-S - entrance 5-slit assembly, GP - ground plate, HVP - high voltage plate, G - grid, D - detector.

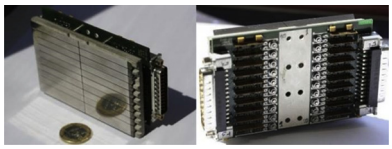

Fig. 6. Beam detector assembly for 5 spatial channels. Left: front view – beam detector; right: back view – preamplifiers for 20 electronic channels.

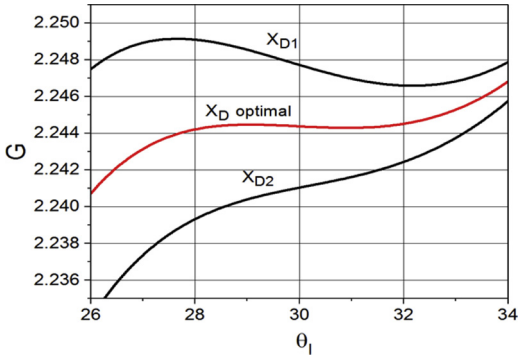

Fig. 7. Gain function optimization by detector position X_D adjustment $X_{D1} < X_{D\ opt} < X_{D2}$.

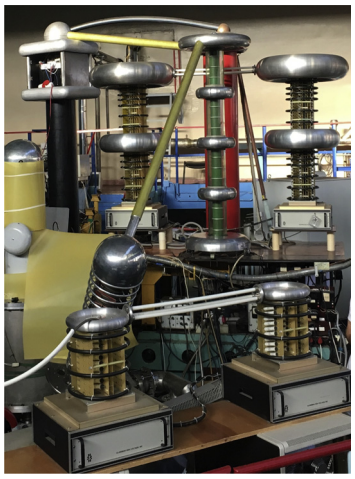

Fig. 8. HIBP on T-10.

keep the uniformity of the analyzing electric field. The cylindrical vacuum vessel of the analyzer is reinforced by stiffening ribs to provide satisfactory rigidity at a low weight. The entrance slit assembly and the beam detector are adjusted with respect to the ground plate with an

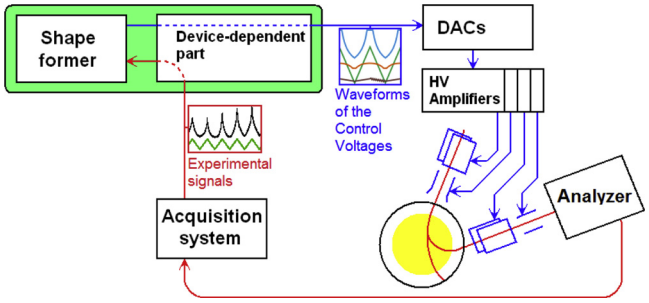

Fig. 9. Scheme of data acquisition and control system.

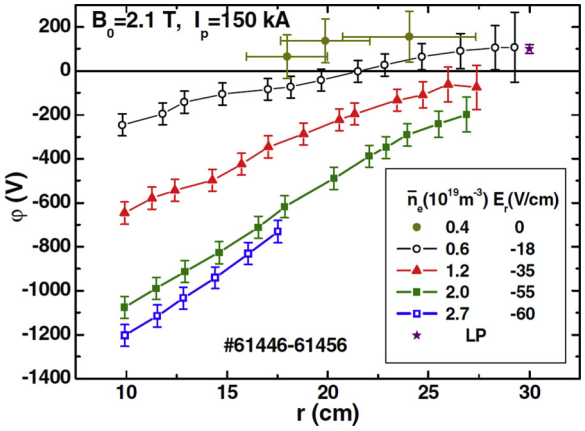

Fig. 10. Potential profile evolution with density.

accuracy of 0.1 mm to avoid instrumental $z - \varphi$ coupling. In addition, ground and anode plates were designed to provide highly homogeneous analyzing electric field.

Fig. 6 shows split-plate detector assembly combined with vacuum-compatible high gain (10^7V/A) preamplifiers, providing the lowest possible parasitic capacitance and 500 kHz bandwidth. The position of the detector assembly X_D is adjusted in order to optimize the dependence of analyzer gain on the entrance angle of the secondary beam into the analyzer $G(\theta_i)$, as presented in Fig. 7. The multichannel energy analyzer allows us the correlation studies between plasma potentials and densities, measured in neighboring sample volumes.

For example, the cross-phase between potentials in poloidally aligned sample volumes provides the poloidal structure of GAM [15]. Simultaneous measurements of density and potential in two poloidally separated points give a unique opportunity to retrieve the electrostatic turbulent particle flux [16].

2.5. HIBP power supply

The open-air accelerator power supply is located at the top of T-10 iron core, it consists of the following parts: 400 kV voltage generator, by Glassman Inc.; capacitive filter to suppress voltage modulation; 1 GΩ measuring divider; insulated high-voltage platform with current source for emitter heating—two 12 V × 120 A·h batteries and two 10 kV voltage sources for three-electrode lens in the emitter-extractor unit. Power sources are controlled via optical line. The analyzer power supply (100 kV voltage generator, by Glassman Inc.) is shown in the foreground of Fig. 8. The main issue in the operation of the high-voltage power supplies is the risk of the corona discharge followed by electrical breakdown. To reduce the risk, all high-voltage ends are covered by anti-corona shaped electrodes. At the closest gaps between the high-voltage parts and grounded elements, the latter were additionally shielded by a thin layer insulator.

High-voltage generators for 400 kV and 100 kV provide necessary

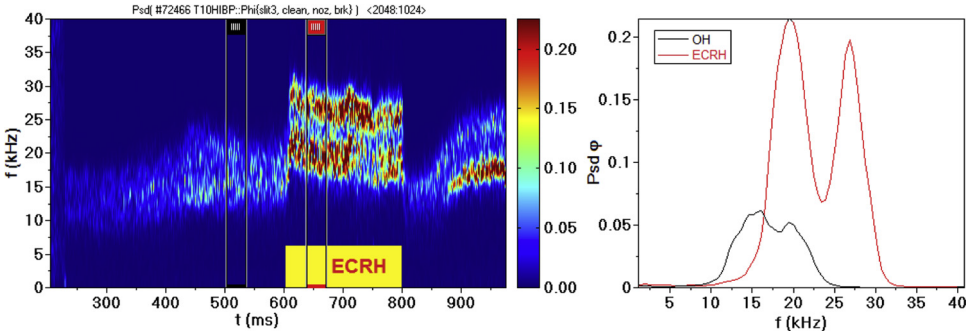

Fig. 11. Power spectrogram (left) and power spectral density (right) of potential oscillation showing GAM evolution with ECRH.

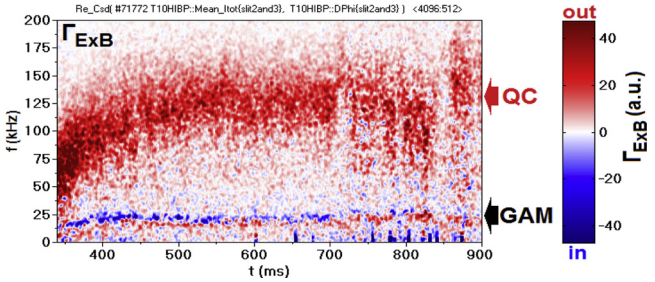

Fig. 12. Spectral function of the turbulent particle flux.

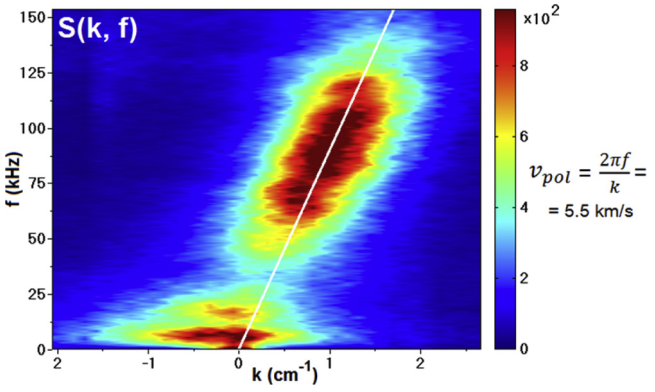

Fig. 13. $S(k, f)$ power spectrum for density perturbation. The white line corresponds to poloidal rotation in the ion diamagnetic drift direction.

voltage stability ($\Delta U/U < 10^{-5}$). Commercial high-voltage amplifiers Trek 30 kV/30 mA and 20 kV/20 mA are used for the plates in beamlines.

2.6. Data acquisition and control system

Data acquisition and control system is based on commercial PXI boards by National Instruments. It has 48 parallel differential ADC channels with 1 MHz sampling frequency. Experimental data from the energy analyzer are stored at the PXI in the torus hall and then sent to the control room PC (Fig. 9). Four arbitrary control voltage waveforms are created by piecewise smooth cubic Bezier curves. The shape former allows us to vary signal shape freely, and then a device-dependent unit sends it via DACs to HV amplifiers (Treks).

3. HIBP operation and physical results

HIBP routinely operates in the whole operational limits of T-10: $1.5 < B_0 < 2.5$ T, $\bar{n}_e = (0.3 - 5) \times 10^{19}$ m^{-3}, $100 < I_{pl} < 330$ kA, in Ohmic and ECRH plasmas using Tl^+ with $E_b < 330$ kV, beam current up to 130 μA.

The HIBP has a unique capability to measure the mean value of the core plasma potential φ, along with the oscillations in φ, n_e and B_{pol} simultaneously in 5 spatially separated SVs [17]. Fig. 10 shows plasma potential profiles taken shot by shot by variation of beam energy E_b from 90 keV to 220 keV. Radial and signal reference was done by Langmuir probe data. Figure shows that plasma with higher density has more negative plasma potential [18]. Fig. 11 shows plasma potential oscillations power spectrogram with a pronounced GAM [19]. In ECRH phase, both GAM amplitude and frequency f_{GAM} rise, and f_{GAM} follows to theoretical scaling $f_{GAM} \sim T_e^{1/2}$ [20].

Fig. 12 presents spectral function of the turbulent particle flux [21] measured in the core plasma. It shows that the main contributor to the outward flux is quasicoherent (QC) mode [22], while GAM contribution is small [23]. 2D frequency-space power spectra $S(k, f)$ of the density oscillations indicate the plasma poloidal rotation with the main contribution of the QC-mode (Fig. 13).

4. Conclusions

The compact HIBP routinely operates in the whole range of T-10 parameters in OH and ECRH plasmas allowing measuring the evolution of potential mean profile, and electrostatic and electromagnetic turbulence characteristics up to 500 kHz.

Acknowledgments

The work is funded by Russian Science Foundation, project 14-22-00193. AVM was partly supported by the Competitiveness Program of NRNU MEPhI.

References

[1] G. Van Oost, et al., Plasma Phys. Control. Fusion 49 (2007) A29.
[2] A.V. Melnikov, Nature Physics 12 (2016) 386.
[3] T.P. Crowley, IEEE Trans. Plasma Sci. 22 (1994) 291.
[4] K.A. Connor, et al., Rev. Sci. Instrum. 63 (1992) 4505.
[5] A. Fujisawa, et al., IEEE Trans. Plasma Sci. 22 (1994) 395.
[6] I.S. Bondarenko, et al., Rev. Sci. Instrum. 72 (2001) 583.
[7] A.V. Melnikov, et al., Rev. Sci. Instrum. 66 (1995) 317.
[8] F.C. Jobes, R.L. Hickock, Nucl. Fusion 10 (1970) 19.
[9] Yu.N. Dnestrovskij, et al., IEEE Trans. Plasma Sci. 22 (1994) 310.
[10] H. Weisen, et al., Fusion Sci. Technol. 59 (2011) 418.
[11] A.V. Melnikov, et al., Nucl. Fusion 57 (2017) 115001.
[12] L.I. Krupnik, et al., IEEE Trans. Plasma Sci. IEEE Nucl. Plasma Sci. Soc. 36 (2008) 1536.
[13] A.V. Melnikov, et al., IEEE Trans. Plasma Sci. IEEE Nucl. Plasma Sci. Soc. 22 (1994) 363.
[14] L. Solensten, K.A. Connor, Rev. Sci. Instrum. 58 (1987) 516.
[15] A.V. Melnikov, et al., Nucl. Fusion 55 (2015) 063001.
[16] L.G. Eliseev, et al., Probl. At. Sci. Technol. Ser.: Plasma Phys. 23 (2017) 241.
[17] A.V. Melnikov, et al., Plasma Phys. Control. Fusion 60 (2018) 084008.
[18] A.V. Melnikov, et al., Nucl. Fusion 53 (2013) 093019.
[19] A.V. Melnikov, et al., Plasma Phys. Control. Fusion 48 (2006) S87.
[20] A. Fujisawa, et al., Nucl. Fusion 47 (2007) S718.
[21] E.J. Powers, Nucl. Fusion 14 (1974) 74.
[22] A.V. Vershkov, et al., Nucl. Fusion 55 (2015) 063014.
[23] L.G. Eliseev, et al., J. Phys. Conf. Ser. 907 (2017) 012002.